STRUCTURAL CONTROL AND HEALTH MONITORING
Struct. Control Health Monit. 2011; **18**:519–539
Published online 6 April 2010 in Wiley Online Library (wileyonlinelibrary.com). DOI: 10.1002/stc.388

A numerical method for the time-domain dynamic analysis of buildings equipped with viscoelastic dampers

Alessandro Palmeri[1,2,*,†] and Giuseppe Muscolino[3,4]

[1]*School of Engineering, Design and Technology, University of Bradford, U.K.*
[2]*Department of Civil and Building Engineering, Loughborough University, U.K.*
[3]*Department of Civil Engineering, University of Messina, Italy*
[4]*Inter-University Centre of Theoretical and Experimental Dynamics, University of Messina, Italy*

SUMMARY

A novel numerical scheme for the time-domain dynamic analysis of buildings incorporating energy dissipation devices of viscoelastic type is presented. Two alternative state-space representations are considered for the frequency-dependent behaviour of the viscoelastic dampers, namely generalized Maxwell's (GM) model and Laguerre's polynomial approximation (LPA) technique. The computational burden is dramatically reduced by using a convenient modal transformation of coordinates, where the equilibrium modulus of the viscoelastic devices is included in the evaluation of modal shapes and undamped modal frequencies. Both GM model and LPA technique lead to closed-form expressions for the parameters characterizing the modal relaxation functions of the building, which in turn are exploited in deriving the exact integration operators for the modal oscillators. Importantly, all the matrices required in the proposed cascade scheme are directly computable from the exact transition matrices of traditional state variables (displacements and velocities) and additional internal variables (for either GM model or LPA technique). A simple application to a Single-DoF oscillator demonstrates the unconditional stability of the numerical method; the numerical efficiency is proved with the dynamic analysis of a discretized structural system with a large number of degrees of freedom; the accuracy is confirmed by the seismic response analysis of a realistic 10-storey building equipped with viscoelastic dampers. Copyright © 2010 John Wiley & Sons, Ltd.

Received 18 January 2009; Revised 1 December 2009; Accepted 2 February 2010

KEY WORDS: energy dissipation devices; generalized Maxwell's model; Laguerre's polynomial approximation technique; numerical scheme; state-space equations; viscoelastic dampers

1. INTRODUCTION

A vast computational and experimental literature has been devoted in the last two decades to structural applications of viscoelastic dampers [1–7]. Indeed, these devices prove to be very effective in mitigating the dynamic impact of natural actions such as ground shakings, wind gusts and ocean waves. Despite recent advances in the field, very crude approximations are often exploited by structural engineers in practical situations, which contrast with the extraordinary rheological complexity of elastomeric materials used in viscoelastic dampers [8–12]. The most popular techniques of analysis and design are based on the Modal Strain Energy (MSE) method, in which effective values of elastic stiffness and viscous damping are utilized. Originally

*Correspondence to: Alessandro Palmeri, Department of Civil and Building Engineering, Loughborough University, U.K.
†E-mail: a.palmeri@lboro.ac.uk, dynamics.structures@gmail.com

developed for laminated composites containing viscoelastic layers [13,14], this approach has been subsequently adapted to seismic and wind applications [15–17]. Although very straightforward, the MSE method may lead to unacceptable inaccuracies in many engineering situations, as demonstrated by recent investigations conducted in different contexts [18–23].

The problem then exists to develop effective numerical schemes of dynamic analysis to overcome the misleading notion of effective stiffness and damping for the elastomeric devices [24], without excessively increasing the computational effort. Even within the limits of the linear range, in fact, the vibration of buildings equipped with viscoelastic dampers is ruled in the time domain by a quite cumbersome set of second-order integro-differential equations with memory kernels, which requires specialized algorithms.

The computational techniques developed in recent years to address this problem can be classified into two main categories. The first type of strategies consists in the modification of standard numerical schemes. Aprile and Benedetti [25] proposed to couple the Newmark's β method [26] with an additional set of differential equations governing the time evolution of the internal state variables associated with a number of Maxwell's elements. A similar approach is formulated in Patlashenko *et al.* [27], where more sophisticated numerical schemes are considered (e.g. the Hilber–Hughes–Taylor method [28]).

The alternative state-space models independently proposed by Palmeri *et al.* [29] and by Adhikari and Wagner [30,31] constitute the second type of strategies. In these methods, the viscoelastic memory is taken into account by appending to the traditional state variables, i.e. displacements and velocities, a certain number of suitable additional internal variables. The forces experienced by the viscoelastic components are then expressed as linear combination of the new state variables, which are ruled by linear differential equations. As shown in Section 2, where generalized Maxwell's (GM) model and Laguerre's polynomial approximation (LPA) technique are compared, the form of these additional state equations depends on the mathematical representation of the constitutive law for the viscoelastic behaviour. In both the cases, the integro-differential equations of motion are turned into a set of linear differential equations of greater order, but easier to solve. The numerical solution is finally sought for the fully coupled state-space equations.

The main disadvantage of the latter strategies is the excessive number of internal state variables, which may be required in real applications. As an example, the number of devices installed in each storey of a viscoelastically damped building can vary from 1 to 50, or even more. As a result, the number of additional state variables for each storey can be easily much greater than the number of dynamically significant degrees of freedom (DoF).

It follows that, similar to the classical eigenvalue analysis for viscously damped structures, it is necessary to implement a technique able to reduce the size of the matrices for actual buildings provided with viscoelastic devices. Indeed, modal frequencies and modal damping ratios are *de facto* insufficient to characterize the vibration of such structures in the modal space, but the concept of modal decoupling is still valid. Inaudi and Kelly [32] tackled this problem in the frequency domain, providing expressions for diagonalizable frequency-dependent stiffness and damping matrices. The same concept of defining non-viscously damped modal oscillators underlies the introduction of the so-called modal relaxation functions in the time domain. As in Palmeri *et al.* [19], for studying the wind-induced vibration of viscoelastically damped buildings, the modal relaxation functions can be viewed as the time-domain counterpart of the frequency-dependent stiffness and damping matrices appearing in the frequency domain.

Aimed at reducing the computational effort of time-domain dynamic analyses, two main novelties are introduced in this study. First, new closed-form expressions are provided in Section 3, which enable the mechanical parameters of the modal relaxation functions to be computed starting from the analogous quantities of the viscoelastic dampers. These formulae are specialized for both GM model and LPA technique. Secondly, an improved cascade scheme of solution is formulated in Section 4. This further innovation is obtained through convenient manipulations of the coupled state-space equations of motion, which make all the approximate integration operators directly computable from the transition matrices of traditional state variables and additional internal variables.

DOI: 10.1002/stc

Three numerical examples are presented in Section 5 for validation purposes. The unconditional stability of the proposed numerical scheme is checked with reference to a Sigle-DoF viscoelastic oscillator with a Maxwell's rheological element. The numerical efficiency is demonstrated with the dynamic analysis of a finite element (FE) model with a large number of DoFs. Finally, practical effectiveness and accuracy are confirmed by the seismic application to a realistic 10-storey building equipped with viscoelastic dampers.

2. CONSTITUTIVE LAW FOR LINEAR VISCOELASTIC DEVICES

Within the limits of the linear theory, the reaction force $r(t)$ experienced by a viscoelastic device can be expressed in the time domain through a convolution integral [18]:

$$r(t) = \varphi(t) * \dot{q}(t) = \int_{-\infty}^{+\infty} \varphi(t-s)\dot{q}(s)\,\mathrm{d}s, \tag{1}$$

where asterisk and over-dot stand for convolution operator and time derivative, respectively; $q(t)$ is the time history of the pertinent deformation of the viscoelastic device; and $\varphi(t)$ is its relaxation function, i.e. the time history of the reaction force due to a unit-step deformation applied for $t = 0$. In practical situations, the function $\varphi(t)$ is non-negative and monotonically decreasing for $t \geqslant 0$ (Figure 1, left); moreover, $\varphi(t)$ must be zero for $t < 0$ to satisfy the causality constraint. The latter condition, along with the assumption that the device is unloaded for $t \leqslant 0$, allows to simplify Equation (1) as:

$$r(t) = \int_0^t \varphi(t-s)\,\dot{q}(s)\,\mathrm{d}s = K_0 q(t) + \int_0^t g(t-s)\dot{q}(s)\,\mathrm{d}s, \tag{2}$$

where K_0 is the equilibrium modulus of the viscoelastic device, representing its purely elastic stiffness and $g(t)$ the time-varying part the relaxation function $\varphi(t)$, that is (Figure 1, right):

$$K_0 = \lim_{t\to\infty} \varphi(t) = \varphi(\infty), \quad g(t) = \varphi(t) - \varphi(\infty). \tag{3}$$

The equilibrium modulus K_0 can be easily identified, as a simple static test is only required to determine the horizontal asymptote of the relaxation function of a given viscoelastic device (Figure 1).

2.1. GM model

For many engineering purposes, the dynamic behaviour of a linear viscoelastic device can be accurately approximated by means of the GM model. This rheological model is made of an elastic spring, $\bar{K}_0$, in parallel with a certain number $\bar{\ell}$ of Maxwell's elements, each one given by an elastic spring, $\bar{K}_i$, in series with a viscous dashpot, $\bar{C}_i = \bar{K}_i\bar{\tau}_i$, with $i = 1, \ldots, \bar{\ell}$. The ratio $\bar{\tau}_i = \bar{C}_i/\bar{K}_i$ is the relaxation time of the ith Maxwell's element, which measures the velocity of the unloading process for this rheological unit. One can easily prove [29] that $K_0 = \bar{K}_0 = \varphi(\infty)$ is the equilibrium modulus in the GM model, while the time-varying part of its relaxation function is given by the superposition of $\bar{\ell}$ exponentially decaying functions:

$$\bar{g}(t) = \sum_{i=1}^{\bar{\ell}} \bar{K}_i \exp\left(-\frac{t}{\bar{\tau}_i}\right), \tag{4}$$

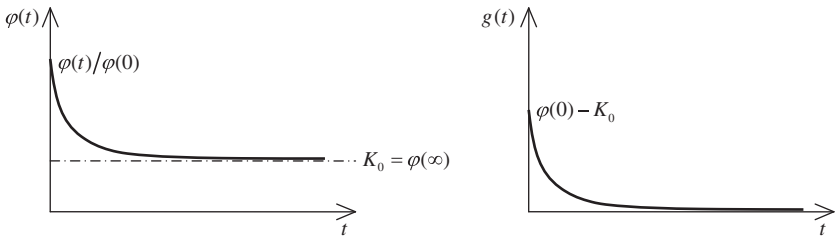

Figure 1. Typical relaxation function $\varphi(t)$ of a viscoelastic damper (left) and its time-varying part $g(t)$ in which the equilibrium modulus K_0 has been removed (right).

DOI: 10.1002/stc

where the over-bar herein denotes the quantities specifically associated with the GM model for a given viscoelastic device.

The experimental identification of the $\bar{\ell}$ pairs or parameters $\{\bar{K}_1, \bar{\tau}_1\}, \ldots, \{\bar{K}_{\bar{\ell}}, \bar{\tau}_{\bar{\ell}}\}$ of the GM model proves to be quite complicated in real applications. The most popular approach consists in a non-linear regression in the frequency domain, based on the results of small-amplitude vibration tests [33,34]. Unfortunately, this is an ill-posed problem, and the numerical solution is fraught with difficulties.

It has been shown that the reaction force of the GM model can be conveniently expressed in the form [29]:

$$\bar{r}(t) = K_0\, q(t) + \sum_{i=1}^{\bar{\ell}} \bar{K}_i\, \lambda_i(t), \tag{5}$$

where the ith additional variable $\lambda_i(t)$, taken as the internal deformation in the ith Maxwell's spring, is ruled by a first-order linear differential equation:

$$\dot{\lambda}_i(t) = \dot{q}(t) - \frac{\lambda_i(t)}{\bar{\tau}_i}. \tag{6}$$

2.2. LPA technique

In Palmeri *et al.* [29], a novel technique, termed LPA, has been proposed for representing the relaxation function of a viscoelastic device with the help of the ortho-normal properties of the Laguerre's polynomials. Accordingly, the approximate time-dependent part of the relaxation function is given by a single exponentially decaying function modulated by a polynomial of order $\tilde{\ell}$ (i.e. an expression alternative to Equation (4) for the GM model):

$$\tilde{g}(t) = \exp\left(-\frac{t}{\tilde{\tau}_0}\right) \sum_{i=1}^{\tilde{\ell}} \tilde{K}_i L_{i-1}\left(\frac{t}{\tilde{\tau}_0}\right), \tag{7}$$

where the over-tilde denotes the quantities specifically associated with the LPA technique for a given viscoelastic device; $\tilde{\tau}_0$ is a characteristic relaxation time of the viscoelastic device; and $\tilde{K}_i$ is the ith Laguerre's rigidity, with $i = 1, \ldots, \tilde{\ell}$. The parameter $\tilde{\tau}_0$ can be easily estimated from a single relaxation test, e.g. through the procedure described in Reference [29], while:

$$\tilde{K}_i = \frac{1}{\tilde{\tau}_0} \int_0^{+\infty} g(t) L_{i-1}\left(\frac{t}{\tilde{\tau}_0}\right) \mathrm{d}t. \tag{8}$$

The function $L_p(\cdot)$ in Equations (7) and (8) stands for the pth Laguerre's polynomial, which for $p \geqslant 2$ can be evaluated as:

$$L_{p+1}(x) = \frac{2p+1-x}{p+1} \mathrm{L}_p(x) - \frac{p}{p+1} \mathrm{L}_{p-1}(x), \tag{9}$$

being $L_0(x) = 1$ and $L_1(x) = 1 - x$.

In Reference [29], it is also shown that the reaction force in the LPA technique turns out to be (alternative to Equation (5)):

$$\tilde{r}(t) = K_0 q(t) + \sum_{i=1}^{\tilde{\ell}} \tilde{K}_i\, \lambda_i(t), \tag{10}$$

where again $K_0 = \varphi(\infty)$ is the equilibrium modulus; and again the ith additional internal variable $\lambda_i(t)$ is ruled by a first-order linear differential equation (alternative to Equation (6)):

$$\dot{\lambda}_i(t) = \dot{q}(t) - \frac{1}{\tilde{\tau}_0} \sum_{j=1}^{i} \lambda_j(t). \tag{11}$$

DOI: 10.1002/stc

It is worth noting that, although formally similar, some important differences exist between GM model and LPA technique: (i) just one characteristic relaxation time $\tilde{\tau}_0$ has to be defined in the LPA technique, while the number $\bar{\ell}$ of relaxation times in the GM model cannot be a priori specified; (ii) the $\tilde{\ell}$ Laguerre's rigidities $\tilde{K}_1, \ldots, \tilde{K}_{\ell}$ can be evaluated from a single relaxation test by using Equation (8), while the rigidities $\bar{K}_1, \ldots, \bar{K}_{\ell}$ have to be identified along with the corresponding relaxation times $\bar{\tau}_1, \ldots, \bar{\tau}_{\ell}$ from many vibrations tests; (iii) the time evolution of the ith additional internal variable $\lambda_i(t)$ in the LPA technique involves all the first i internal variables (Equation (11)), while in the GM model, all the internal variables are uncoupled (Equation (6)), i.e. loading and unloading processes of the Maxwell's elements are independent.

3. STATE-SPACE EQUATIONS OF MOTION FOR STRUCTURAL SYSTEMS INCORPORATING VISCOELASTIC DEVICES

The dynamic equilibrium of a linear building structure, having n DoF and r added linear viscoelastic dampers (Figure 2, left), is governed in the time domain by a set of n-coupled integro-differential equations of second order:

$$\mathbf{M} \cdot \ddot{\mathbf{u}}(t) + \mathbf{C} \cdot \dot{\mathbf{u}}(t) + \mathbf{K} \cdot \mathbf{u}(t) + \sum_{j=1}^{r} \mathbf{b}_j \cdot \int_0^t \varphi_j(t-s) \mathbf{b}_j^{\mathrm{T}} \cdot \dot{\mathbf{u}}(s)\, \mathrm{d}s = \mathbf{f}(t), \tag{12}$$

where $\mathbf{M}$, $\mathbf{C}$ and $\mathbf{K}$ are the matrices of mass, damping and stiffness of the structural system without viscoelastic devices, respectively; the jth kernel $\varphi_j(t)$ is the relaxation function of the jth viscoelastic damper; $\mathbf{b}_j$ is its influence vector; and $\mathbf{f}(t)$ is the array of the time-varying external forces acting on the building; while a dot is used to denote the matrix product.

3.1. Modal analysis

Following the modal analysis proposed by Palmeri *et al.* [19], let us consider the transformation of coordinates:

$$\mathbf{u}(t) = \mathbf{\Phi} \cdot \mathbf{q}(t) = \sum_{k=1}^{m} \boldsymbol{\phi}_k q_k(t), \tag{13}$$

where the rectangular modal matrix $\mathbf{\Phi} = [\boldsymbol{\phi}_1 \cdots \boldsymbol{\phi}_m]$, of dimensions $m \times n$, and the m-dimensional array $\mathbf{q}(t) = \{q_1(t) \cdots q_m(t)\}^{\mathrm{T}}$ collect the first $m \leqslant n$ modal shapes and the corresponding modal coordinates of the building structure, respectively (in real applications, $m \ll n$). The kth modal shape, $\boldsymbol{\phi}_k$, is evaluated along with the corresponding undamped natural

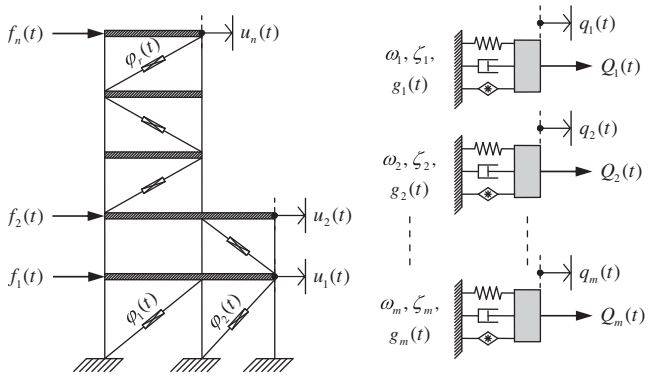

Figure 2. Framed structure equipped with viscoelastic dampers (left) and associated modal oscillators (right), in which the asterisked diamonds denote the time-varying part of the modal relaxation functions.

DOI: 10.1002/stc

circular frequency, ω_k, as solution of the real-valued eigenproblem:

$$\begin{aligned} &\left[\mathbf{K}+\sum_{j=1}^{r}\mathbf{b}_j\cdot\mathbf{b}_j^{\mathrm{T}}\varphi_j(\infty)\right]\cdot\boldsymbol{\phi}_k=\omega_k^2\mathbf{M}\cdot\boldsymbol{\phi}_k,\\ &\boldsymbol{\phi}_i^{\mathrm{T}}\cdot\mathbf{M}\cdot\boldsymbol{\phi}_k=\delta_{i,k}, \end{aligned} \tag{14}$$

$\delta_{i,k}$ being the Kronecker's delta symbol, equal to one when $i=k$, zero otherwise. Interestingly, the summation in the left-hand side of the first of Equations (14) accounts for the additional stiffness arising in static conditions (i.e. when the circular frequency of vibration ω goes to zero) from the introduction of the viscoelastic dampers.

Pre-multiplying Equation (12) by $\boldsymbol{\Phi}^{\mathrm{T}}$, one obtains the integro-differential equations of motion in the reduced modal space:

$$\ddot{\mathbf{q}}(t)+\boldsymbol{\Xi}\cdot\dot{\mathbf{q}}(t)+\boldsymbol{\Omega}^2\cdot\mathbf{q}(t)+\int_0^t\mathbf{G}(t-s)\cdot\dot{\mathbf{q}}(s)\,\mathrm{d}s=\boldsymbol{\Phi}^{\mathrm{T}}\cdot\mathbf{f}(t), \tag{15}$$

where $\boldsymbol{\Xi}=\boldsymbol{\Phi}^{\mathrm{T}}\cdot\mathbf{C}\cdot\boldsymbol{\Phi}$ is the reduced viscous damping matrix, associated with the inherent dissipation of the building without viscoelastic dampers; $\boldsymbol{\Omega}=\mathrm{diag}\{\omega_1\cdots\omega_m\}$ is the spectral matrix of the structure, which includes the increase in the stiffness due to the equilibrium modulus of the viscoelastic dampers; and $\mathbf{G}(t)$ is the modal relaxation matrix, taking into account the time-varying part of the viscoelastic kernels, that is:

$$\mathbf{G}(t)=\boldsymbol{\Phi}^{\mathrm{T}}\cdot\left[\sum_{j=1}^{r}\mathbf{b}_j\cdot\mathbf{b}_j^{\mathrm{T}}(\varphi_j(t)-\varphi_j(\infty))\right]\cdot\boldsymbol{\Phi}. \tag{16}$$

For homogeneous structural systems, it is often assumed that the modal shapes are orthogonal with respect not only to mass and stiffness matrices, **M** and **K**, but also with respect to the viscous damping matrix, **C**. For instance, this is the usual way of mathematically representing the small amount of energy dissipation provided by internal frictions in both steel and reinforced concrete frames. When this condition is met, the structure is said to be classically (or proportionally) damped, and the equations of motion turn out to be decoupled in terms of modal coordinates [35]. This important result can be extended to the case of buildings in which the viscoelastic dampers are distributed almost homogeneously, e.g. somehow proportionally to the floor masses and/or to the rigidities of the structural frame [16,17,21,32]. Analytically, this extension implies to neglect the off-diagonal elements of the relaxation matrix $\mathbf{G}(t)$:

$$\mathbf{G}(t)=\mathrm{diag}\{g_1(t)\ldots g_m(t)\}. \tag{17}$$

It would be important to emphasize that this assumption is far from being unrealistic. Starting from the pioneering installation in the Twin Towers of the World Trade Center in New York (1969), in fact, viscoelastic dampers are generally distributed almost homogeneously over the resisting structure [1,4]. The aim is to spread the energy dissipation in as many locations as possible, which is what typically happens for many engineering applications. For the sake of completeness, the general mathematical conditions to perfectly decouple the equations of motion in the modal space are provided in Appendix A.

3.2. Uncoupled modal equations of motion

Once the matrices $\boldsymbol{\Xi}$ and $\mathbf{G}(t)$ in Equation (15) are assumed to be diagonal, the transformation of coordinates of Equation (13) can be used to decouple the equations of motion in the reduced modal space, so that the kth modal coordinate $q_k(t)$ is ruled by:

$$\ddot{q}_k(t)+2\zeta_k\omega_k\dot{q}_k(t)+\omega_k^2q_k(t)+\int_0^t g_k(t-s)\dot{q}_k(s)\,\mathrm{d}s=Q_k(t), \tag{18}$$

DOI: 10.1002/stc

in which kth modal excitation and kth modal relaxation function are given by:

$$\begin{aligned} Q_k(t) &= \boldsymbol{\phi}_k^{\mathrm{T}} \cdot \mathbf{f}(\mathrm{t}), \\ g_k(t) &= \boldsymbol{\phi}_k^{\mathrm{T}} \cdot \left[\sum_{j=1}^{r} \mathbf{b}_j \cdot \mathbf{b}_j^{\mathrm{T}} (\varphi_j(t) - \varphi_j(\infty)) \right] \cdot \boldsymbol{\phi}_k = \sum_{j=1}^{r} \gamma_{k,j} (\varphi_j(t) - \varphi_j(\infty)), \end{aligned} \tag{19}$$

where the combination coefficient $\gamma_{k,j} = \boldsymbol{\phi}_k^{\mathrm{T}} \cdot \mathbf{b}_j \cdot \mathbf{b}_j^{\mathrm{T}} \cdot \boldsymbol{\phi}_k$ represents the influence of the jth viscoelastic damper on the kth modal relaxation function.

Interestingly, Equation (18) can be viewed as the integro-differential equation governing the motion of the kth modal oscillator of the building structure. As schematically illustrated in Figure 2 (right), this is made of a unit mass restrained by an elastic spring ω_k^2 in parallel with a viscous dashpot $2\zeta_k\omega_k$ and with an additional viscoelastic device of relaxation function $g_k(t)$, having zero equilibrium modulus (fluid-like behaviour), the pure elastic contribution of the viscoelastic dampers being included in ω_k^2.

As the relaxation function $\varphi(t)$ of a real viscoelastic device can be represented by using either GM model or LPA technique, the same can be carried out for the modal relaxation function $g_k(t)$. More precisely, from the comparison between Equation (2) and either Equation (5) for the GM model or Equation (10) for the LPA technique, it follows that the convolution integral appearing in Equation (18) can be turned into:

$$\int_0^t g_k(t-s)\, \dot{q}_k(s)\, \mathrm{d}s = \sum_{i=1}^{\ell} \beta_{k,i} \lambda_{k,i}(t), \tag{20}$$

where ℓ is the number of additional internal variables used for each modal oscillator; and the coefficient $\beta_{k,i}$ plays the same role as the rigidities $\bar{K}_i$ and $\tilde{K}_i$ in Equations (5) and (10), and thus in principle could be identified in the same way. Analogously, the additional internal variable $\lambda_{k,i}(t)$ is ruled by the same type of linear differential equations presented in the previous section for GM model (Equation (6)) and LPA technique (Equation (11)), depending on the approximation used for the modal relaxation function. The resulting equations are explicitly presented in the Sections 3.3 and 3.4.

Upon substitution of Equation (20) into Equation (18), the dynamic response of the kth modal oscillator can be posed in a state-space form, which is independent of the modelling used for $g_k(t)$:

$$\dot{\mathbf{x}}_k(t) = \mathbf{D}_k \cdot \mathbf{x}_k(t) + \mathbf{B}_k \cdot \boldsymbol{\lambda}_k(t) + \mathbf{v} Q_k(t), \tag{21}$$

where $\mathbf{x}_k(t) = \{q_k(t)\ \dot{q}_k(t)\}^{\mathrm{T}}$ is the two-dimensional array of the usual state variables, i.e. the modal displacement $q_k(t)$ and the modal velocity $\dot{q}_k(t)$; $\boldsymbol{\lambda}_k(t) = \{\lambda_{k,1}(t) \cdots \lambda_{k,\ell}(t)\}^{\mathrm{T}}$ is the ℓ-dimensional array listing the additional state variables associated with the approximate modal relaxation function; and

$$\mathbf{D}_k = \begin{bmatrix} 0 & 1 \\ -\omega_k^2 & -2\zeta_k\omega_k \end{bmatrix}, \quad \mathbf{B}_k = -\begin{bmatrix} 0 & 0 & \cdots & 0 \\ \beta_{k,1} & \beta_{k,2} & \cdots & \beta_{k,\ell} \end{bmatrix}, \quad \mathbf{v} = \begin{Bmatrix} 0 \\ 1 \end{Bmatrix}. \tag{22}$$

On the contrary, the rate of variation of the new state array $\lambda_k(t)$ is ruled by:

$$\dot{\boldsymbol{\lambda}}_k(t) = \hat{\mathbf{D}} \cdot \boldsymbol{\lambda}_k(t) + \mathbf{A} \cdot \mathbf{x}_k(t), \tag{23}$$

where the ℓ-dimensional matrix $\hat{\mathbf{D}}$ is defined in the following subsections for both GM model and LPA technique; and the matrix $\mathbf{A}$, of dimensions $\ell \times 2$, is in both the cases:

$$\mathbf{A} = \begin{bmatrix} 0 & 0 & \cdots & 0 \\ 1 & 1 & \cdots & 1 \end{bmatrix}^{\mathrm{T}}. \tag{24}$$

It is worth highlighting here that in Equation (23), the hat distinguishes the matrix of coefficients for the additional internal variables, $\hat{\mathbf{D}}$, from that one for the classical state variables, $\mathbf{D}_k$, which appears in Equation (21). Moreover, matrices $\hat{\mathbf{D}}$ and $\mathbf{A}$ are the same for all the modal oscillators.

DOI: 10.1002/stc

3.3. GM model

If the GM model is used for all the viscoelastic dampers incorporated into the building structure, then the relaxation times $\{\bar{\tau}_{j,1},\ldots,\bar{\tau}_{j,\bar{\ell}_j}\}$ of the jth device are also relaxation times of the modal oscillators. Accordingly, the full set of modal relaxation times is so defined:

$$\{\tau_1,\ldots,\tau_\ell\} = \bigcup_{j=1}^{r} \{\bar{\tau}_{j,1},\ldots,\bar{\tau}_{j,\bar{\ell}_j}\}, \tag{25}$$

where the $\bigcup$ stands for the union operator; and $\bar{\ell}_j$ and ℓ (with $\bar{\ell}_j \leqslant \ell$) are the numbers of Maxwell's elements in the jth viscoelastic damper and in each modal oscillator, respectively. By particularizing the second of Equation (19) for the GM model (Equation (4)), one obtains:

$$g_k(t) = \sum_{j=1}^{r} \gamma_{k,j}\bar{g}_j(t) = \sum_{j=1}^{r} \gamma_{k,j} \sum_{i=1}^{\bar{\ell}_j} \bar{K}_{j,i} \exp\left(-\frac{t}{\bar{\tau}_{j,i}}\right), \tag{26}$$

where $\bar{g}_j(t) = \varphi_j(t) - \varphi_j(\infty)$ is the time-varying part of the GM-type relaxation function for the jth viscoelastic damper; and $\bar{K}_{j,i} = \bar{K}_j(\bar{\tau}_{j,i})$ is its discrete relaxation spectrum, whose ordinate $\bar{K}_{j,i}$ represents the elastic stiffness of the ith Maxwell's element having relaxation time $\bar{\tau}_{j,i}$. Taking into account Equation (25), the order of the summations in Equation (26) can be reversed, and the expression so obtained can be further simplified as:

$$g_k(t) = \sum_{i=1}^{\ell} \sum_{j=1}^{r} \gamma_{k,j} \bar{K}_j(\tau_i) \exp\left(-\frac{t}{\tau_i}\right) = \sum_{i=1}^{\ell} \beta_{k,i} \exp\left(-\frac{t}{\tau_i}\right), \tag{27}$$

where $\beta_{k,i}$ is the ith element appearing in the second row of the matrix $\mathbf{B}_k$ introduced in Equations (21) and (22), which takes the exact expression:

$$\beta_{k,i} = \sum_{j=1}^{r} \gamma_{k,j} \bar{K}_j(\tau_i). \tag{28}$$

By virtue of the formal similarity with Equation (4), the generic exponential function appearing in the right-hand side of Equation (27) can be associated with the additional internal variable $\lambda_{k,i}(t)$, in which the subscripts k and i denote modal oscillator and relaxation time, respectively. It follows that this new state variable is ruled by a linear differential equation formally similar to Equation (6):

$$\dot{\lambda}_{k,i}(t) = \dot{q}_k(t) - \frac{\lambda_{k,i}(t)}{\tau_i}, \tag{29}$$

so that the matrix of coefficients $\hat{\mathbf{D}}$ in Equation (23) takes the diagonal form:

$$\hat{\mathbf{D}} = -\begin{bmatrix} \tau_1^{-1} & & & \\ & \tau_2^{-1} & & \\ & & \ddots & \\ & & & \tau_\ell^{-1} \end{bmatrix}, \tag{30}$$

which is the same for all the modal oscillators. Interestingly, this method of projecting the relaxation functions of the viscoelastic dampers onto the reduced modal space does not introduce further approximations in the dynamic analysis of the building, as the expressions of Equations (25)–(30) are exact.

3.4. LPA technique

If the LPA technique is used for all the viscoelastic dampers incorporated into the building, considering in all the cases the same characteristic relaxation time τ_0 and the same number of terms ℓ, then these values can also be assumed for all the modal oscillators. Indeed, by particularizing the second of Equation (19) for the LPA technique (Equation (7)), one obtains

DOI: 10.1002/stc

(analogous and alternative to Equation (26)):

$$g_k(t) = \sum_{j=1}^{r} \gamma_{k,j} \tilde{g}_j(t) = \sum_{j=1}^{r} \gamma_{k,j} \exp\left(-\frac{t}{\tau_0}\right) \sum_{i=1}^{\ell} \tilde{K}_{j,i} L_{i-1}\left(\frac{t}{\tau_0}\right), \tag{31}$$

where $\tilde{K}_{j,i}$ is the ith Laguerre's rigidity for the jth viscoelastic damper. By reversing the order of the summation, and further simplifying the expression so obtained, Equation (31) gives:

$$g_k(t) = \sum_{i=1}^{\ell} \sum_{j=1}^{r} \gamma_{k,j} \tilde{K}_{j,i} L_{i-1}\left(\frac{t}{\tau_0}\right) \exp\left(-\frac{t}{\tau_0}\right) = \exp\left(-\frac{t}{\tau_0}\right) \sum_{i=1}^{\ell} \beta_{k,i} L_{i-1}\left(\frac{t}{\tau_0}\right), \tag{32}$$

with the following position (similar to Equation (28)) for the coefficients appearing in the matrix $\mathbf{B}_k$ introduced in Equations (21) and (22):

$$\beta_{k,i} = \sum_{j=1}^{r} \gamma_{k,j} \tilde{K}_{j,i}. \tag{33}$$

By taking advantage of the formal similarity with Equation (7), the generic Laguerre's polynomial appearing in the right-hand side of Equation (32) can be associated with the additional internal variable $\lambda_{k,i}(t)$, in which the subscripts k and i denote modal oscillator and order of the polynomial, respectively. It follows that this new state variable is ruled by a linear differential equation formally similar to Equation (11):

$$\dot{\lambda}_{k,i}(t) = \dot{q}_k(t) - \frac{1}{\tau_0} \sum_{j=1}^{i} \lambda_{k,j}(t), \tag{34}$$

so that the ℓ-dimensional matrix of coefficients $\hat{\mathbf{D}}$ in Equation (23) takes the lower-triangular form:

$$\hat{\mathbf{D}} = -\tau_0^{-1} \begin{bmatrix} 1 & & & \\ 1 & 1 & & \\ \vdots & \vdots & \ddots & \\ 1 & 1 & \cdots & 1 \end{bmatrix}, \tag{35}$$

which is the same for all the modal oscillators.

4. NUMERICAL METHOD OF SOLUTION

In the previous sections, GM model and LPA technique have been reviewed for a single viscoelastic device, and then extended to cope with viscoelastically damped buildings in the modal space. Aim of this section is to formulate a numerical scheme for the time-domain dynamic analysis of such type of structural systems.

To do this, let the time axis be subdivided into small intervals of equal length, Δt, which in practical applications must satisfy the two conditions:

$$\Delta t \leqslant \min\left\{\frac{\pi}{4 \max\{\omega_m, \omega_c\}}, \frac{1}{3}\tau_{\min}\right\}, \tag{36}$$

where ω_m is the undamped circular frequency of the higher mode of vibration retained in the analysis; ω_c the cut-off frequency of the external excitation; and $\tau_{\min}$ the shortest relaxation time considered among the r viscoelastic dampers. These conditions make sure that all the non-negligible harmonic contributions to the structural response and all the relaxation processes of the viscoelastic dampers are represented with sufficient accuracy in the numerical solution.

Under the assumption that the inhomogeneous terms in Equations (21) and (23) vary linearly in each time step, the numerical solution for the kth modal oscillator can be posed in the

DOI: 10.1002/stc

incremental form [36–38]:

$$\begin{aligned}\mathbf{x}_k(t+\Delta t) &= \boldsymbol{\Theta}_k \cdot \mathbf{x}_k(t)+\boldsymbol{\Gamma}'_k \cdot \{\mathbf{v}Q_k(t)+\mathbf{B}_k \cdot \boldsymbol{\lambda}_k(t)\}+\boldsymbol{\Gamma}''_k \cdot \{\mathbf{v}Q_k(t+\Delta t)+\mathbf{B}_k \cdot \boldsymbol{\lambda}_k(t+\Delta t)\},\\ \boldsymbol{\lambda}_k(t+\Delta t) &= \hat{\boldsymbol{\Theta}} \cdot \boldsymbol{\lambda}_k(t)+\hat{\boldsymbol{\Gamma}}' \cdot \mathbf{A} \cdot \mathbf{x}_k(t)+\hat{\boldsymbol{\Gamma}}'' \cdot \mathbf{A} \cdot \mathbf{x}_k(t+\Delta t),\end{aligned} \tag{37}$$

where the explicit dependence on the time step Δt of the integration operators (i.e. the matrices $\boldsymbol{\Theta}$ and $\boldsymbol{\Gamma}$) has been omitted to simplify the notation; and $\boldsymbol{\lambda}_k$ is handled as an array of pseudo-forces acting on the state-space array $\mathbf{x}_k$ and vice versa.

The integration operators in the first of Equations (37), without the hat, are those evaluated from $\mathbf{D}_k$, which is the classical matrix of coefficients of a single-DoF oscillator with viscous damping. More precisely, $\boldsymbol{\Theta}_k$ is the transition matrix of the kth modal oscillator for the selected time step Δt, which is known in closed form:

$$\boldsymbol{\Theta}_k = \exp[\mathbf{D}_k \Delta t] = \begin{bmatrix} \cos(\Omega_k \Delta t)+\dfrac{\zeta_k \omega_k}{\Omega_k}\sin(\Omega_k \Delta t) & \dfrac{1}{\Omega_k}\sin(\Omega_k \Delta t) \\ -\dfrac{\omega_k^2}{\Omega_k}\sin(\Omega_k \Delta t) & \cos(\Omega_k \Delta t)-\dfrac{\zeta_k \omega_k}{\Omega_k}\sin(\Omega_k \Delta t) \end{bmatrix} \exp(-\zeta_k \omega_k \Delta t), \tag{38}$$

the reduced circular frequency Ω_k being:

$$\Omega_k = \sqrt{1-\zeta_k^2}\,\omega_k. \tag{39}$$

The other two integration operators appearing in the right-hand side of the first of Equations (37) are given by:

$$\boldsymbol{\Gamma}'_k = \left[\boldsymbol{\Theta}_k - \frac{1}{\Delta t}\mathbf{L}_k\right] \cdot \mathbf{D}_k^{-1}, \quad \boldsymbol{\Gamma}''_k = \left[\frac{1}{\Delta t}\mathbf{L}_k - \mathbf{I}_2\right] \cdot \mathbf{D}_k^{-1}, \tag{40}$$

where the $\mathbf{I}_s$ stands for the identity matrix of size s, while

$$\mathbf{L}_k = [\boldsymbol{\Theta}_k - \mathbf{I}_2] \cdot \mathbf{D}_k^{-1}, \quad \mathbf{D}_k^{-1} = \begin{bmatrix} -2\zeta_k \omega_k^{-1} & -\omega_k^{-2} \\ 1 & 0 \end{bmatrix}. \tag{41}$$

In the second of Equations (37), the ℓ-dimensional transition matrix $\hat{\boldsymbol{\Theta}}$, associated with the additional internal variables through the matrix of coefficients $\hat{\mathbf{D}}$, can also be evaluated in closed form for both GM model and LPA technique, and the relative expressions are provided in the following subsections. Once the transition matrix $\hat{\boldsymbol{\Theta}}$ is known, the dependant matrices $\hat{\boldsymbol{\Gamma}}'$ and $\hat{\boldsymbol{\Gamma}}''$ can be computed as (analogously to Equations (40)):

$$\hat{\boldsymbol{\Gamma}}' = \left[\hat{\boldsymbol{\Theta}} - \frac{1}{\Delta t}\hat{\mathbf{L}}\right] \cdot \hat{\mathbf{D}}^{-1}, \quad \hat{\boldsymbol{\Gamma}}'' = \left[\frac{1}{\Delta t}\hat{\mathbf{L}} - \mathbf{I}_\ell\right] \cdot \hat{\mathbf{D}}^{-1}, \tag{42}$$

in which (analogous to the first of Equation (41)):

$$\hat{\mathbf{L}} = [\hat{\boldsymbol{\Theta}} - \mathbf{I}_\ell]\,\hat{\mathbf{D}}^{-1}. \tag{43}$$

The computation of the inverse matrix $\hat{\mathbf{D}}_k^{-1}$ is possible in closed form as well, as the matrix of coefficient $\hat{\mathbf{D}}_k$ has a very special form for both GM model and LPA technique. The respective inverse matrices are provided in the Sections 4.1 and 4.2.

The inspection of Equations (37) reveals that the two state arrays $\mathbf{x}_k$ and $\boldsymbol{\lambda}_k$ are coupled, as the traditional state variables at the end of the time step, listed in $\mathbf{x}_k(t+\Delta t)$, depend on the additional state variables at the same instant, listed in $\boldsymbol{\lambda}_k(t+\Delta t)$, and vice versa. As a matter of fact, this coupling does not allow evaluating the exact integration operators of the viscoelastic modal oscillators in closed form. However (Appendix B), a new form can be derived by manipulating

DOI: 10.1002/stc

Equations (37), which enables an alternative, and very effective, solution in cascade:

$$\begin{aligned}\mathbf{x}_k(t+\Delta t) &= \breve{\mathbf{\Theta}}_k \cdot \mathbf{x}_k(t)+\breve{\mathbf{\Psi}}_k \cdot \boldsymbol{\lambda}_k(t)+\{\breve{\mathbf{\Gamma}}'_k \cdot \mathbf{v}\}Q_k(t)+\{\breve{\mathbf{\Gamma}}''_k \cdot \mathbf{v}\}Q_k(t+\Delta t),\\ \boldsymbol{\lambda}_k(t+\Delta t) &= \breve{\mathbf{\Theta}}_k \cdot \boldsymbol{\lambda}_k(t)+[\hat{\mathbf{\Gamma}}' \cdot \mathbf{A}] \cdot \mathbf{x}_k(t)+[\breve{\mathbf{\Gamma}}'' \cdot \mathbf{A}] \cdot \mathbf{x}_k(t+\Delta t),\end{aligned} \tag{44}$$

where the over-arc denotes the updated terms in the first of Equations (44), which are so defined:

$$\begin{aligned}\breve{\mathbf{\Theta}} &= \mathbf{E}_k \cdot [\mathbf{\Theta}_k+\mathbf{\Gamma}''_k \cdot \mathbf{B}_k \cdot \hat{\mathbf{\Gamma}}' \cdot \mathbf{A}], \quad \breve{\mathbf{\Psi}}_k = \mathbf{E}_k \cdot [\mathbf{\Gamma}'_k \cdot \mathbf{B}_k+\mathbf{\Gamma}''_k \cdot \mathbf{B}_k \cdot \hat{\mathbf{\Theta}}],\\ \breve{\mathbf{\Gamma}}'_k &= \mathbf{E}_k \cdot \mathbf{\Gamma}'_k, \quad \breve{\mathbf{\Gamma}}''_k = \mathbf{E}_k \cdot \mathbf{\Gamma}''_k,\end{aligned} \tag{45}$$

$\mathbf{E}_k$ being a modification matrix of dimensions 2×2:

$$\mathbf{E}_k = [\mathbf{I}_2 - \mathbf{\Gamma}''_k \cdot \mathbf{B}_k \cdot \hat{\mathbf{\Gamma}}'' \cdot \mathbf{A}]^{-1}. \tag{46}$$

Assuming that the building structure is at rest for $t \leqslant 0$, i.e. $\mathbf{x}_k(0)$ and $\boldsymbol{\lambda}_k(0)$ are nil arrays, the numerical scheme starts solving the cascade Equations (44) for $t = 0$:

$$\begin{aligned}\mathbf{x}_k(\Delta t) &= \breve{\mathbf{\Gamma}}'_k \cdot \mathbf{v}Q_k(0)+\breve{\mathbf{\Gamma}}''_k \cdot \mathbf{v}Q_k(\Delta t),\\ \boldsymbol{\lambda}_k(\Delta t) &= \hat{\mathbf{\Gamma}}'' \cdot \mathbf{A} \cdot \mathbf{x}_k(\Delta t).\end{aligned} \tag{47}$$

The scheme then continues, step by step, with the cascade Equations (44) for $t = \Delta t, 2\Delta t, \ldots$, until the final time instant $t_f = N\Delta t$ is reached, N being the number of the sampling time instants.

Before proceeding with the specialized expressions of transition matrix $\hat{\mathbf{\Theta}}$ and inverse of $\hat{\mathbf{D}}$ for both GM model (Section 4.1) and LPA techniques (Section 4.2), it is may be useful to stress the practical advantages of a cascade numerical scheme. First, the evaluation of the integration operators for the fully coupled differential equations of motions is avoided, in so saving computational time. Secondly, in each time step the dynamic equilibrium and the loading/unloading processes of the viscoelastic components (first and second of Equations (44), respectively) are decoupled. This can simplify, for instance, the application of re-analysis techniques for optimization purposes [39,40], as modifications in the viscoelastic dampers do not affect the integration operators associated with the classical state variables of the building; moreover, nonlinear phenomena in the structural frame and/or in the elastomeric devices can be handled separately.

4.1. GM model

The cascade scheme formulated in the earlier section requires the transition matrices for classical state variables ($\mathbf{\Theta}_k$) and additional internal variables ($\hat{\mathbf{\Theta}}$). These fundamental integration operators are defined as the matrix exponential of the respective matrices of coefficients, $\mathbf{D}_k$ and $\hat{\mathbf{D}}$. The first operator is given by Equation (38), while the second one depends on the mathematical representation of the viscoelastic memory. When the GM model is used, the matrix of coefficient $\hat{\mathbf{D}}$ is diagonal (Equation (30)), and hence also the associated transition matrix $\hat{\mathbf{\Theta}}$ takes a diagonal form:

$$\hat{\mathbf{\Theta}} = \exp[\hat{\mathbf{D}}\Delta t] = \begin{bmatrix} \exp(-\Delta t/\tau_1) & & & \\ & \exp(-\Delta t/\tau_2) & & \\ & & \ddots & \\ & & & \exp(-\Delta t/\tau_\ell) \end{bmatrix}. \tag{48}$$

DOI: 10.1002/stc

The matrix inverse of $\hat{\mathbf{D}}$, which is also required (Equations (42) and (43)), is also diagonal:

$$\hat{\mathbf{D}}^{-1} = -\begin{bmatrix} \tau_1 & & & \\ & \tau_2 & & \\ & & \ddots & \\ & & & \tau_\ell \end{bmatrix}. \tag{49}$$

4.2. LPA technique

When the LPA technique is used, the matrix of coefficients $\hat{\mathbf{D}}$ is lower triangular, filled with τ_0^{-1} (Equation (35)), and therefore, the correspondent transition matrix $\hat{\mathbf{\Theta}}$ is also lower triangular, and depends on the dimensionless ratio $\alpha = \Delta t/\tau_0$ only:

$$\hat{\mathbf{\Theta}} = \exp[\hat{\mathbf{D}}\Delta t] = \begin{bmatrix} P_1(\alpha) & & & \\ P_2(\alpha) & P_1(\alpha) & & \\ \vdots & \vdots & \ddots & \\ P_{\ell_k}(\alpha) & P_{\ell_k-1}(\alpha) & \cdots & P_1(\alpha) \end{bmatrix} \exp(-\alpha), \tag{50}$$

in which $P_1(\alpha) = 1$, while the higher-order polynomials $P_2(\alpha), \ldots, P_\ell(\alpha)$ are given by the recursive expression:

$$P_i(\alpha) = -\sum_{j=1}^{i-1} \int_0^\alpha P_j(\rho)\, \mathrm{d}\rho. \tag{51}$$

The first polynomials so computed are listed below:

$$\begin{aligned} &P_2(\alpha) = -\alpha, \quad P_3(x) = -\alpha + \frac{\alpha^2}{2}, \quad P_4(\alpha) = -\alpha + \alpha^2 - \frac{\alpha^3}{6}, \\ &P_5(\alpha) = -\alpha + \frac{3}{2}\alpha^2 - \frac{\alpha^3}{2} + \frac{\alpha^4}{24}, \quad P_6(\alpha) = -\alpha + 2\alpha^2 - \alpha^3 + \frac{\alpha^4}{6} - \frac{\alpha^5}{120}, \ldots \end{aligned} \tag{52}$$

The inverse matrix of $\hat{\mathbf{D}}$ proves to be lower-bidiagonal, and it is simply given by:

$$\hat{\mathbf{D}}^{-1} = -\tau_0 \begin{bmatrix} 1 & & & \\ -1 & 1 & & \\ & \ddots & \ddots & \\ & & -1 & 1 \end{bmatrix}. \tag{53}$$

5. NUMERICAL VALIDATION

5.1. Numerical stability

Aim of this section is to investigate the numerical stability of the scheme of solution proposed in the earlier section. Without lack of generality, the numerical stability can be studied by considering the free vibration of a generic modal oscillator [25–28]. By neglecting the modal excitation $Q_k(t)$, after a simple manipulation, Equations (44) can be rearranged in the compact form:

$$\left\{\begin{matrix} \mathbf{x}(t+\Delta t) \\ \dot{\mathbf{x}}(t+\Delta t) \end{matrix}\right\} = \left[\begin{array}{c|c} \mathbf{\Theta} & \mathbf{\Psi} \\ \hline \hat{\mathbf{\Gamma}}' \cdot \mathbf{A} + \hat{\mathbf{\Gamma}}'' \cdot \mathbf{A} \cdot \breve{\mathbf{\Theta}} & \hat{\mathbf{\Theta}} + \hat{\mathbf{\Gamma}}'' \cdot \mathbf{A} \cdot \breve{\mathbf{\Psi}} \end{array}\right] \cdot \left\{\begin{matrix} \mathbf{x}(t) \\ \dot{\mathbf{x}}(t) \end{matrix}\right\}, \tag{54}$$

where the subscript k is omitted to simplify the notation; and the block matrix into square brackets is the amplification matrix of the numerical scheme. This matrix depends on the selected time step Δt along with the mechanical properties of the modal oscillator. When the viscous damping is

DOI: 10.1002/stc

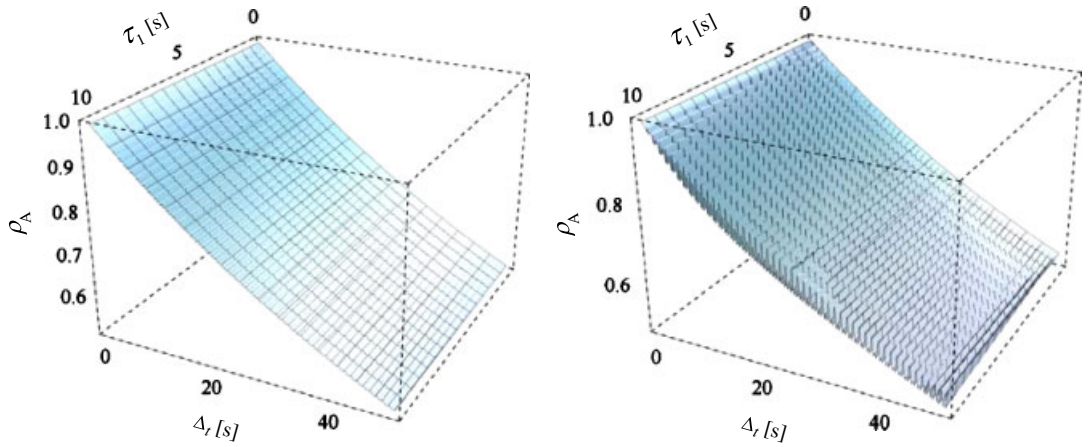

Figure 3. Spectral radius ρ_A of the proposed numerical scheme as a function of time step Δt and relaxation time τ_1 for low (left) and high (right) viscoelastic damping.

considered in parallel with the viscoelastic relaxation, one can verify that the resulting amplification matrix tends to the identity matrix when $\Delta t \to 0$, and to the nil matrix when $\Delta t \to +\infty$. The latter condition proves that the amplification matrix is asymptotically stable.

For an arbitrary time step $0 < \Delta t < +\infty$, the stability of the numerical solution can be directly related to the spectral radius of the amplification matrix, ρ_A, which is defined as the supremum among the moduli of its eigenvalues. For a given time step Δt, in fact, $\rho_A < 1$ is a sufficient condition for the numerical stability.

To verify with an example that the proposed scheme of solution is unconditionally stable, i.e. stable for any time step Δt, the spectral radius ρ_A for a modal oscillator with a single Maxwell's element has been studied. The undamped period of vibration and the viscous damping ratio are chosen as $T = 2\pi/\omega = 1\,\mathrm{s}$ and $\zeta = 0.002$; two values of the stiffness parameters $\beta_1 = 1\,\mathrm{s}^{-2}$ and $\beta_1 = 10\,\mathrm{s}^{-2}$ are considered; the relaxation time τ_1 and the time step Δt vary in the intervals $[0, 10\,\mathrm{s}]$ and $[0, 50\,\mathrm{s}]$, respectively. Figure 3 displays the spectral radius of the amplification matrix ρ_A as a function of τ_1 and Δt for the two selected values of β_1, representative of low and high viscoelastic damping. In both the cases, $\rho_A < 1$ for $\Delta t > 0$, i.e. the numerical algorithm is stable, and in both the cases ρ_A tends to decrease when Δt increases. The comparison between the graphs obtained for $\beta_1 = 1\,\mathrm{s}^{-2}$ and $\beta_1 = 10\,\mathrm{s}^{-2}$ reveals that in the second case, the spectral radius shows some fluctuations, which however do not affect the numerical stability of the proposed method of dynamic analysis.

5.2. Numerical efficiency

As far as the computational efficiency is concerned, the performances of the proposed approach have been compared with those of the numerical scheme formulated by Patlashenko *et al.* [27]. The objective structural system is the slender cantilever beam shown in Figure 4, which is 1.00 m long, 0.10 m deep and 0.20 m wide. The material constituting the beam is assumed to be purely elastic, without inherent damping. Young's modulus and Poisson's coefficient take the values $E = 300\,\mathrm{MPa}$ and $\nu = 0.20$, respectively, while the mass density is $\rho = 1500\,\mathrm{kg/m^3}$. Energy dissipation is provided by a set of viscoelastic strips perfectly bonded to the beam (2 longitudinal and 20 inclined by 45°), which are represented through linear viscoelastic springs connecting the joints of the FE model of the beam (Figure 4). The equilibrium modulus of a strip 1-m long is $K_0 = 2000\,\mathrm{kN/m}$, while the time varying part of the relaxation function is described by $\bar{\ell} = 3$ Maxwell's elements, whose mechanical parameters are listed in Table I. The FE mesh of the beam consists of $Q = 10M^2$ plane-stress four-node quadrilateral elements [41] with unit aspect ratio (square shape), M being the number of elements in the transverse direction of the beam (M is equal to 4 in Figure 4). The mesh has been progressively refined by taking $M = 1$, 2, 4, 8 and 16. For these five cases, the number of quadrilateral elements (Q), viscoelastic springs (r) and

DOI: 10.1002/stc

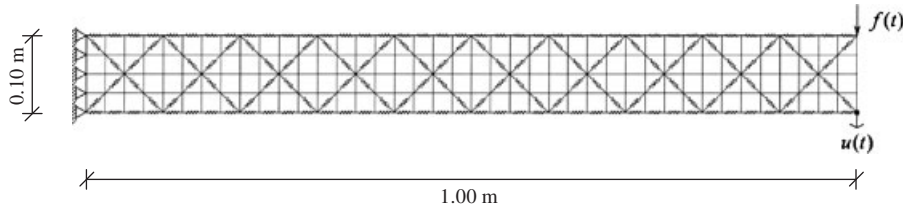

Figure 4. Finite element model of the slender beam with viscoelastic strips considered in the second numerical application.

Table I. Parameters of the Generalized Maxwell's model for the viscoelastic strips considered in the second numerical application.

$\bar{\ell}$	$K_0/\varphi(0)$	$\bar{K}_1/\varphi(0)$	$\bar{\tau}_1$ (s)	$\bar{K}_2/\varphi(0)$	$\bar{\tau}_2$ (s)	$\bar{K}_3/\varphi(0)$	$\bar{\tau}_3$ (s)
3	0.20	0.20	0.010	0.50	0.005	0.10	0.0005

Table II. Different finite element models for the second numerical application.

M	$Q = 10\,\mathrm{M}^2$	$r = 40$ M	$n = 2Q+r/2$	Ω_1 (rad/s)	ω_1 (rad/s)
1	10	40	40	54.0	82.9
	(—)	(—)	(—)	(—)	(—)
2	40	80	120	47.6	80.0
	(+300%)	(+50%)	(+200%)	(−11.9%)	(−3.5%)
4	160	160	400	45.7	79.1
	(+300%)	(+50%)	(+233%)	(−3.9%)	(−1.1%)
8	640	320	1440	45.2	78.8
	(+300%)	(+50%)	(+260%)	(−1.1%)	(−0.4%)
16	2560	640	5440	45.1	78.7
	(+300%)	(+50%)	(+278%)	(−0.2%)	(−0.1%)

DoFs (n) are summarized in Table II, along ith the values of the fundamental frequency of vibration with (ω_1) and without (Ω_1) the application of the viscoelastic strips. The percentage variation of these quantities with the refinement of the mesh is also reported into parentheses. The inspection of Table II reveals that with $M = 8$ subdivisions in the transverse direction (i.e. with $n = 1440$ DoFs), the convergence in terms of fundamental frequency of vibration has been reached for engineering purposes.

The forced vibration of the slender beam under the harmonic force $f(t) = F\sin(\Omega_f t)$, with amplitude $F = 10N$ and circular frequency $\Omega_f = 80\,\mathrm{rad/s}$, has been considered. The force is applied at the top node of the beam's free end, while the dynamic response $u(t)$ has been computed at the bottom node (Figure 5) in the time interval $[0, t_f]$, with $t_f = 0.50\,\mathrm{s}$. For each of the five FE models with different numbers of DoFs, three alternative dynamic analyses have carried out, namely: (A) proposed approach in the reduced modal space, with $m = 5$ modal coordinates retained in the analysis; (B) the numerical scheme presented by Patlashenko *et al.* [27], namely the SIDE (System of Integro-Differential Equations) scheme based on the Newmark's β method with parameters $\beta = 1/4$ and $\gamma = 1/2$ (constant average acceleration method) and with semi-analytical integration rule for the hereditary kernels; (C) the same SIDE scheme of Reference [27] applied in the reduced modal space, as obtained by considering the first $m = 5$ modal shapes of the beam without the proposed modification of the eigenproblem (Equation (14)). All the numerical schemes have been implemented in Mathematica 6.0 codes [42], and the time-domain analyses have been carried out on a Microsoft Windows desktop PC equipped with dual-core AMD Athlon 64 X2 processor at 3.0 GHz and with 2.0 GB of RAM. The selected time step was $\Delta t = 0.1$ ms in all the cases, corresponding to $N = 5000$ time steps for each analysis. Table III shows the computational time for different meshes, i.e. for different numbers of DoFs (from $n = 40$ to $n = 5440$). It clearly emerges that the proposed approach (type A analysis) is always computationally more efficient than the nodal SIDE scheme (Type B

DOI: 10.1002/stc

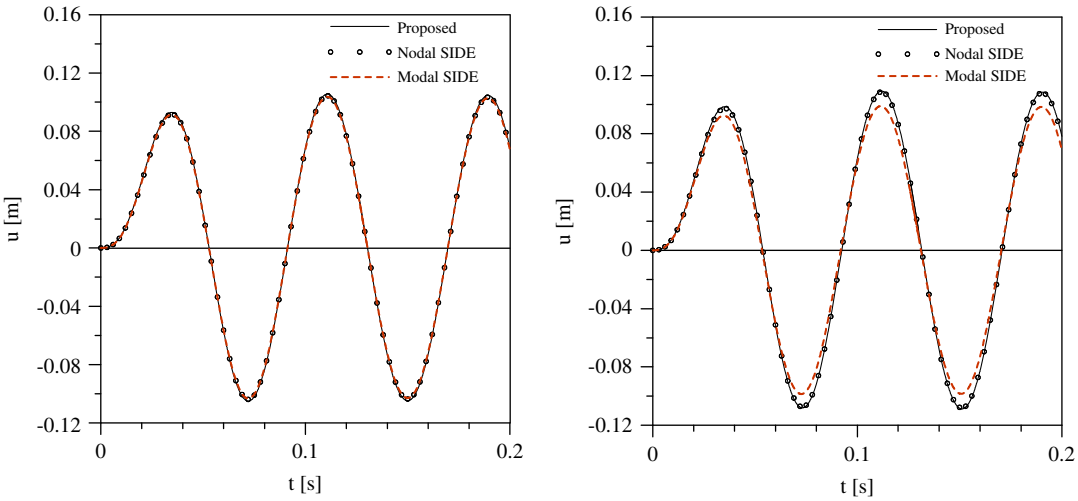

Figure 5. Dynamic response of the slender beam considered in the second numerical application for coarse (left) and fine (right) meshes.

Table III. Computational times required by different analyses for the second numerical application.

n	Type-A analysis (proposed approach) (s)	Type-B analysis (nodal SIDE) (s)	Type-C analysis (modal SIDE) (s)
40	2.3	3.1	1.6
120	2.3	6.1	1.6
400	2.3	21.7	1.8
1440	2.6	87.8	2.5
5440	6.4	425.2	7.7

analysis) presented in Reference [27], and that the advantage increases with the number of DoF. As an example, for $n = 5440$, the computation time reduces from 425.2 s (type B analysis) to 6.4 s (type A analysis). This tremendous improvement is possible by virtue of the proposed modal analysis (Equation (14)), which enables us to reduce the size of the dynamic problem. Indeed, also the SIDE scheme in the conventional modal space (type C analysis) requires computational times similar to those of the proposed approach. However, the inaccuracy of the modal SIDE scheme increases with the number of DoFs, while the proposed approach is always in good agreement with the nodal SIDE scheme. This trend is confirmed by Figure 5, where the results provided by the three numerical schemes are compared for two different FE meshes. For a small number of DoFs ($n = 40$), the discrepancies among the three methods of analysis are virtually indiscernible. On the contrary, for a large number of DoFs ($n = 5440$) proposed approach (thin solid line) and nodal SIDE scheme (reference method, circles) are in good agreement, while the modal SIDE scheme (thick dashed line) significantly underestimates the amplitude of the beam's forced vibration.

5.3. *Realistic building structure*

To test the accuracy of the proposed procedure of analysis in a realistic engineering application, the seismic-induced vibration of the shear-type 10-storey steel frame depicted in Figure 6 (left) has been studied. The values of mass M_i and lateral stiffness of the main frame K_i, taken from Reference [43], are summarized in Table IV, while the inherent viscous damping ratio of the steelwork structure is assumed to be $\zeta_0 = 0.02$.

A single viscoelastic damper is ideally located at each storey, and connected to the principal moment-resisting frame through a very stiff bracing system. Initial value of damper's relaxation function and brace's rigidity at the ith level are 1.2 and 10.0 times greater than the corresponding main stiffness K_i at the same level, respectively. The first three modal shapes of

DOI: 10.1002/stc

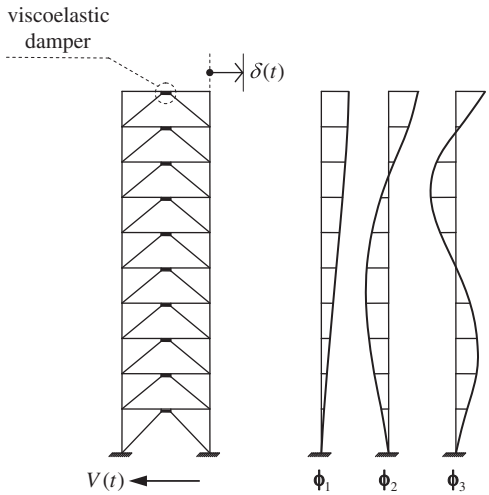

Figure 6. Steel frame considered in the third numerical application (left) and modal shapes retained in the analysis (right).

Table IV. Main characteristics of the steel frame considered in the third numerical application.

Storey level i	Mass M_i (Mg)	Frame stiffness K_i (kN/mm)	Type of viscoelastic damper
10	29.1	4.25	B
9	35.4	5.34	B
8	35.4	6.80	B
7	35.9	7.76	B
6	35.9	8.96	B
5	35.9	10.2	A
4	36.8	11.3	A
3	36.8	12.9	A
2	36.8	13.3	A
1	38.6	14.6	A

Table V. Parameters of the Generalized Maxwell's model for the viscoelastic dampers considered in the third numerical application.

Type	$\bar{\ell}$	$K_0/\varphi(0)$	$\bar{K}_1/\varphi(0)$	$\bar{\tau}_1$ (s)	$\bar{K}_2/\varphi(0)$	$\bar{\tau}_2$ (s)	$\bar{K}_3/\varphi(0)$	$\bar{\tau}_3$(s)
A	2	0.20	0.20	0.15	0.60	0.25	—	—
B	3	0.10	0.30	0.03	0.30	0.06	0.30	0.15

the frame under investigation are displayed in Figure 6 (right), as evaluated including also the effects of bracing system and equilibrium modulus of the viscoelastic dampers (Equation (14)). The associated undamped modal frequencies are $\omega_1 = 2.93$, $\omega_2 = 7.50$ and $\omega_3 = 12.0\,\text{rad/s}$.

Two different types of relaxation functions are considered for bottom and top floors, namely types A and B, which in practice could be given either by a single actual device or by the superposition of many devices installed at the same level. Both type A and type B viscoelastic dampers are represented with the GM model, whose parameters (rigidities and relaxation times) are summarized in Table V. The dimensionless relaxation functions are plotted in Figure 7, whose inspection reveals that the process of relaxation is more rapid in type B devices.

The first three modes of vibration are retained in the analysis ($m = 3$), which ensure that in this case, 94% of the participating mass of the building is included in the analysis (i.e. for seismic applications, the same considerations hold as for conventional buildings with classical viscous damping). Following the exact procedure presented in Section 3.3, three relaxation times are considered for each modal oscillator ($\ell = 3$), and the nine ($m \times \ell = 9$) modal parameters $\beta_{k,i}$ are evaluated in closed form through Equation (28).

DOI: 10.1002/stc

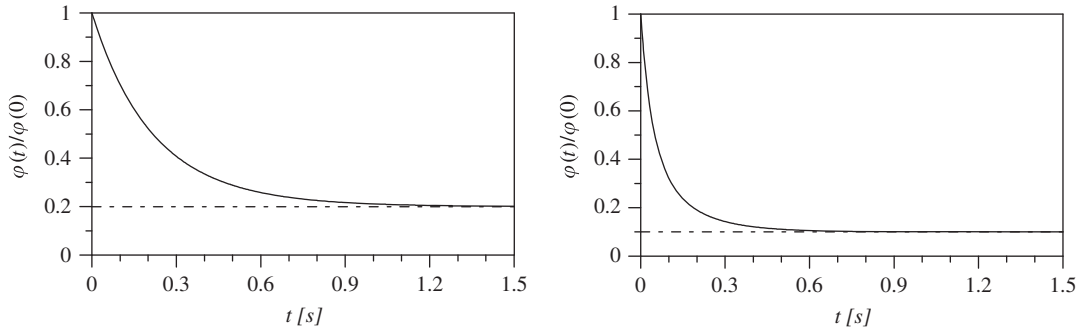

Figure 7. Dimensionless relaxation functions for type A (left) and type B (right) viscoelastic dampers considered in the third numerical application.

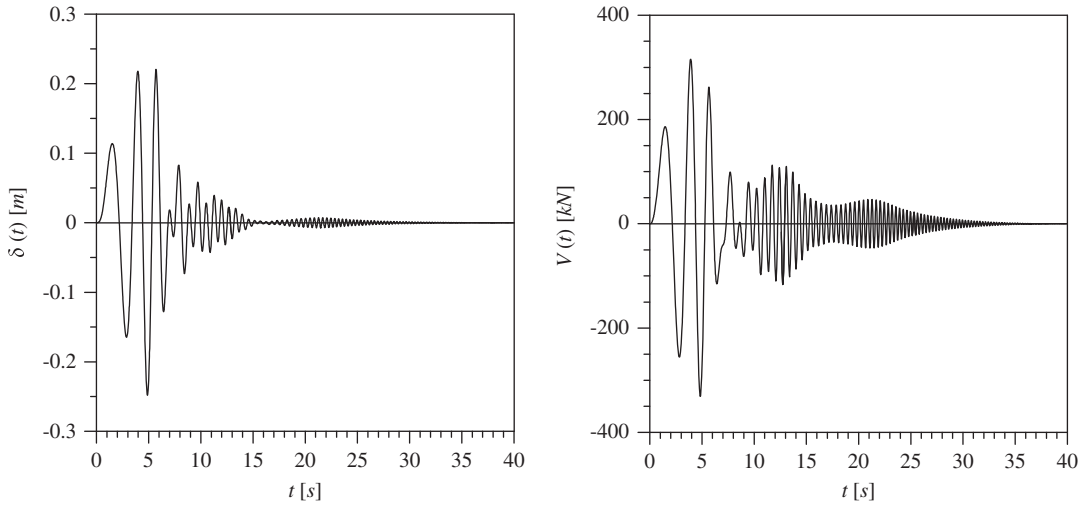

Figure 8. Time histories of tip displacements (left) and base shear (right).

To successively excite the modes of vibration of the building retained in the dynamic analysis, the ground acceleration has been conveniently modelled as a modulated sinusoidal function, $\ddot{u}_g(t) = A_g(t)\sin(\Omega_g(t)\,t)$, where amplitude and frequency of the input are given by $A_g(t) = (1+\sin(\pi t/t_f) - t/t_f)^2$ and $\Omega_g(t) = 1+14t/t_f$, respectively, $t_f = 40\,\mathrm{s}$ being the final time instant.

Figure 8 shows the time histories of tip displacement $\delta(t)$ and base shear $V(t)$ delivered by the proposed numerical scheme. These pictures reveal that the only significant contribution to the tip displacement is due to the first mode of vibration in the first seconds of the motion, while also the second mode contributes to the shear force. The accuracy of the results has been assessed in the frequency domain. The bilogarithmic graphs of Figure 9 compare the modulus of the Fourier's transform of the time histories $\delta(t)$ and $V(t)$ furnished by the proposed dynamic analysis (solid lines) with the corresponding frequency-domain responses (dashed lines) computed through the n-dimensional frequency response function matrix of the system, so defined [24]:

$$\mathbf{H}(\omega) = \left[\omega^2\mathbf{M}+\mathbf{K}+\imath\omega\left[\mathbf{C}+\sum_{j=1}^{r}\mathbf{b}_j\cdot\mathbf{b}_j^{\mathrm{T}}\mathrm{F}\langle\varphi_j(t)\rangle\right]\right]^{-1}, \tag{55}$$

where $\imath = \sqrt{-1}$ is the imaginary unit, F denotes the Fourier transform of the quantity within angle brackets, and the approximate viscous damping matrix is given by $\mathbf{C} \cong 2\zeta_0\,\mathbf{M}\cdot\mathbf{\Phi}\cdot\mathbf{\Omega}\cdot\mathbf{\Phi}^{\mathrm{T}}\cdot\mathbf{M}$. The comparison is very satisfactory, as the proposed numerical scheme is able to perfectly capture all the significant features of the building's dynamics with three modes of vibration only, in so reducing tremendously the computational effort.

DOI: 10.1002/stc

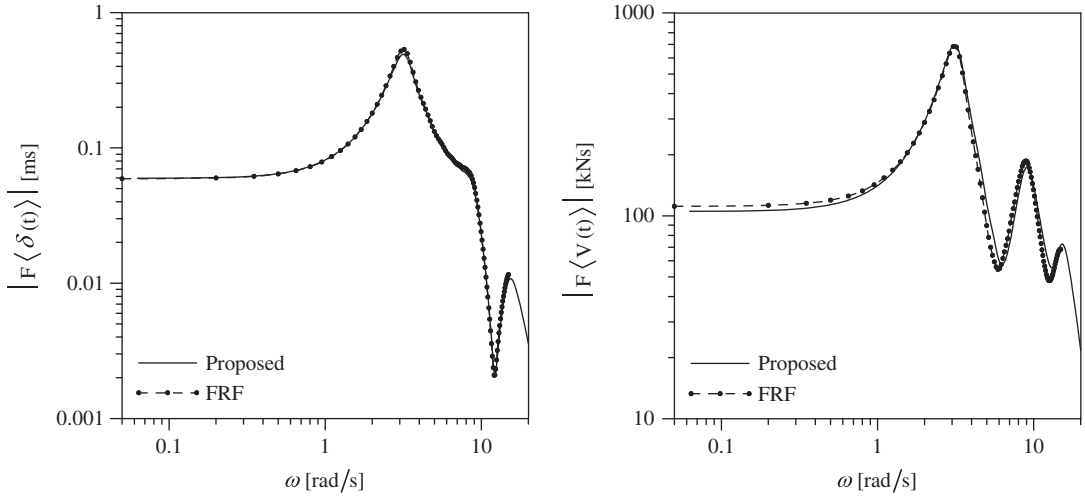

Figure 9. Modulus of the frequency-domain response in terms of tip displacements (left) and base shear (right).

6. CONCLUSIONS AND PERSPECTIVES

In the framework of the dynamic analysis of linear building structures provided with linear viscoelastic dampers, a new numerical scheme of time-domain solution has been presented and validated by examples. The free vibration analysis of a simple Single-DoF oscillator with viscoelastic memory has been used to check the unconditional stability of the method. The improved computational efficiency has been shown through the dynamic analysis of a FE structural model with a large number of DoFs. The accuracy has been demonstrated through the seismic application to a realistic Multi-DoF steel frame equipped with viscoelastic energy dissipation devices.

Among the advantages of the proposed technique: (i) new closed-form expressions are derived for the integration operators when the viscoelastic devices are represented either via GM model or via LPA technique; (ii) operating in the modal space, by means of a novel formulation in cascade, the computational burden is further reduced. These innovations make the proposed numerical scheme absolutely competitive in terms of computational time with the traditional MSE method, whose inaccuracies can become intolerable for engineering applications.

Interestingly, when the LPA technique is adopted, the additional advantage exists that just simple relaxation tests are required for the viscoelastic dampers, in so avoiding more complicated frequency-domain characterizations of the elastomeric materials. On the contrary, the GM model is much more popular in the current state-of-practice, and consequently, this alterative representation of the viscoelastic memory has also been considered in the proposed formulation.

The approach presented in this study lends itself to be extended to cope with more complex structural systems. Future studies may be devoted to consider geometrical and/or material nonlinearities by implementing a re-analysis technique [40] to update, step-by-step, the matrices appearing in the right-hand side of Equation (44). Semi-active control strategies could also be worth of investigation: for instance, by using magneto-rheological braces [44] in series with viscoelastic dampers, one can obtain controllably modal relaxation times, whose effectiveness would be studied numerically and experimentally.

APPENDIX A: MODAL DECOUPLING FOR VISCOELASTICLLAY DAMPED STRUCTURES

The concept of modal coupling for structural systems provided with viscoelastic devices has been rigorously addressed in the frequency domain by Inaudi and Kelly [32]. Similar conclusions can be developed in the time domain. It is well known that, following Caughey and O'Kelly [35], the modal shapes $\boldsymbol{\phi}_k$ delivered by Equation (14) are able to diagonalize the viscous

DOI: 10.1002/stc

damping matrix $\mathbf{C}$ in Equation (12) if and only if this matrix can be written as:

$$\mathbf{C} = \mathbf{M} \cdot \sum_i [\mathbf{M}^{-1} \cdot \mathbf{K}_\infty]^i \, \xi_i, \tag{A1}$$

where ξ_i is a real-valued scalar coefficient, and where $\mathbf{K}_\infty$ is the stiffness matrix in the left-hand side of Equation (14):

$$\mathbf{K}_\infty = \mathbf{K} + \sum_{j=1}^{r} \mathbf{b}_j \cdot \mathbf{b}_j^{\mathrm{T}} \, \varphi_j(\infty). \tag{A2}$$

Interestingly, if ξ_0 and ξ_1 are the only two non-zero coefficients, the viscous damping matrix turns out to be a linear combination of mass and stiffness matrices:

$$\mathbf{C} = \xi_0 \mathbf{M} + \xi_1 \, \mathbf{K}_\infty, \tag{A3}$$

which is the classical case of Rayleigh's damping. It is well known that in the reduced modal space Equation (A3) reduces to:

$$\mathbf{\Xi} = \xi_0 \, \mathbf{I}_m + \xi_1 \mathbf{\Omega}^2. \tag{A4}$$

Analogously to the pure viscous damping, the viscoelastic relaxation terms in the left-hand side of Equation (12) are diagonalizable in the modal space if and only if, for a generic time instant t, the following condition holds:

$$\sum_{j=1}^{r} \mathbf{b}_j \cdot \mathbf{b}_j^{\mathrm{T}} (\varphi_j(t) - \varphi_j(\infty)) = \mathbf{M} \cdot \sum_i [\mathbf{M}^{-1} \cdot \mathbf{K}_\infty]^i \, \eta_i(t), \tag{A5}$$

where $\eta_i(t)$ is a real-valued scalar function of time t. The latter expression can be viewed as time-domain counterpart of those reported by Inaudi and Kelly [32] in the frequency domain, and more recently by Adhikari and Pascual [45] in the Laplace's domain. If both the conditions expressed in Equations (A1) and (A5) are satisfied, then the structural system has uncoupled modes of vibration.

It is worth noting that, similar to the previous case, if $\eta_0(t)$ and $\eta_1(t)$ are the only two non-zero functions in the right-hand side of Equation (A5), then the viscoelastic damping is simply proportional to mass and elastic stiffness. Recalling now Equation (16), this Rayleigh-type viscoelastic damping leads to a very special form of the modal relaxation matrix (analogous to Equation (A4)):

$$\mathbf{G}(t) = \eta_0(t) \, \mathbf{I}_m + \eta_1(t) \mathbf{\Omega}^2. \tag{A6}$$

Indeed, this m-dimensional matrix is diagonal, and its kth element is given by:

$$g_k(t) = \eta_0(t) + \eta_1(t) \, \omega_k^2 \, . \tag{A7}$$

This representation is particularly effective when the structural system is made, for instance, of a single viscoelastic materials.

APPENDIX B: MATHEMATICAL DERIVATION OF THE PROPOSED CASCADE SCHEME

In order to derive the numerical cascade scheme of Equations (44), let us substitute the second of Equations (37) into the first one, in so obtaining the discrete-time relationship:

$$\begin{aligned} \mathbf{x}_k(t+\Delta t) = & \mathbf{\Theta}_k \cdot \mathbf{x}_k(t) + \mathbf{\Gamma}'_k \cdot \{\mathbf{v} \, Q_k(t) + \mathbf{B}_k \cdot \boldsymbol{\lambda}_k(t)\} \\ & + \mathbf{\Gamma}''_k \cdot \{\mathbf{v} Q_k(t+\Delta t) + \mathbf{B}_k \cdot \hat{\mathbf{\Theta}} \cdot \boldsymbol{\lambda}_k(t) + \mathbf{B}_k \cdot \hat{\mathbf{\Gamma}}' \cdot \mathbf{A} \cdot \mathbf{x}_k(t) + \mathbf{B}_k \cdot \hat{\mathbf{\Gamma}}'' \cdot \mathbf{A} \cdot \mathbf{x}_k(t+\Delta t)\}, \end{aligned} \tag{B1}$$

where the traditional two-dimensional state array $\mathbf{x}_k(t+\Delta t)$ at the end of the time step appears in both sides. In order to overcome this inconvenience, Equation (B1) can be rearranged as:

$$\begin{aligned} [\mathbf{I}_2 - \mathbf{\Gamma}''_k \cdot \mathbf{B}_k \cdot \hat{\mathbf{\Gamma}}'' \cdot \mathbf{A}] \cdot \mathbf{x}_k(t+\Delta t) = & [\mathbf{\Theta}_k + \mathbf{\Gamma}''_k \cdot \mathbf{B}_k \cdot \hat{\mathbf{\Gamma}}' \cdot \mathbf{A}] \cdot \mathbf{x}_k(t) \\ & + [\mathbf{\Gamma}'_k \cdot \mathbf{B}_k + \mathbf{\Gamma}''_k \cdot \mathbf{B}_k \cdot \hat{\mathbf{\Theta}}] \cdot \boldsymbol{\lambda}_k(t) + \{\mathbf{\Gamma}'_k \cdot \mathbf{v}\} Q_k(t) + \{\mathbf{\Gamma}''_k \cdot \mathbf{v}\} Q_k(t+\Delta t). \end{aligned} \tag{B2}$$

DOI: 10.1002/stc

Pre-multiplying now both sides of Equation (B1) by the modification matrix of Equation (46), and taking into account the matrices introduced in Equation (45), one obtains the first of Equation (44), in which the state array $\mathbf{x}_k(t+\Delta t)$ at the end of the time step can be predicted by knowing the traditional and additional state variables at the beginning of the time step, $\mathbf{x}_k(t)$ and $\boldsymbol{\lambda}_k(t)$, and knowing also the excitation Q_k at the time instants t and $t+\Delta t$. Once $\mathbf{x}_k(t+\Delta t)$ is evaluated, the array of the additional state variables at the end of the time step can be computed through the second of Equation (44).

REFERENCES

1. Soong TT, Dargush GF. *Passive Energy Dissipation Systems in Structural Engineering*. Wiley: Chichester, 1997.
2. Zhang RH, Soong TT. Seismic design of viscoelastic dampers for structural applications. *Journal of Structural Engineering* 1992; **118**:1375–1392.
3. Tsai CS, Lee HH. Applications of viscoelastic dampers to high-rise buildings. *Journal of Structural Engineering* 1993; **119**:1222–1233.
4. Samali B, Kwok KCS. Use of viscoelastic dampers in reducing wind- and earthquake-induced motion of building structures. *Engineering Structures* 1995; **17**:639–654.
5. Lee HH. Stochastic analysis for offshore structures with added mechanical dampers. *Ocean Engineering* 1997; **24**:817–834.
6. Yang JN, Lin S, Kim, JH, Agrawal AK. Optimal design of passive energy dissipation systems based on H_∞ and H_2 performances. *Earthquake Engineering and Structural Dynamics* 2002; **31**:921–936.
7. Mazza F, Vulcano A. Control of the along-wind response of steel framed buildings by using viscoelastic or friction dampers. *Wind and Structures* 2007; **10**:233–247.
8. Lockett FJ. *Nonlinear Viscoelastic Solids*. Academic Press: London, 1972.
9. Jones DIG. *Handbook of Viscoelastic Vibration Damping*. Wiley: Chichester, 2001.
10. Lesieutre GA, Govindswamy K. Finite element modeling of frequency-dependent and temperature-dependent dynamic behavior of viscoelastic materials in simple shear. *International Journal of Solids and Structures* 1996; **33**:419–432.
11. Johnson AR. Modeling viscoelastic materials using internal variables. *Shock and Vibration Digest* 1999; **31**:91–100.
12. Park SW. Analytical modeling of viscoelastic dampers for structural and vibration control. *International Journal of Solids and Structures* 2001; **38**:8065–8092.
13. Johnson CD, Kienholz DA. Finite element prediction of damping in structures with constrained viscoelastic layers. *AIAA Journal* 1982; **20**:1284–1290.
14. Rao MD, He S. Dynamic analysis and design of laminated composite beams with multiple damping layers. *AIAA Journal* 1993; **31**:736–745.
15. Shen KL, Soong TT, Chang KC, Lai ML. Seismic behaviour of reinforced concrete frame with added viscoelastic dampers. *Engineering Structures* 1995; **17**:372–380.
16. Zambrano A, Inaudi JA, Kelly JM. Modal coupling and accuracy of modal strain energy method. *Journal of Engineering Mechanics* 1996; **122**:603–612.
17. Choa KP, Cermaka JE, Laib ML, Nielsen EJ. Viscoelastic damping for wind-excited motion of a five-story building frame. *Journal of Wind Engineering and Industrial Aerodynamics* 1998; **77–78**:269–281.
18. Palmeri A, Ricciarelli F, De Luca A, Muscolino G. Random vibration of systems with viscoelastic memory. *Journal of Engineering Mechanics* 2004; **130**:1052–1061.
19. Palmeri A, Ricciarelli F, Muscolino G, De Luca A. Effects of viscoelastic memory on the buffeting response of tall buildings. *Wind and Structures* 2004; **7**:89–106.
20. Muscolino G, Palmeri A, Ricciarelli F. Time-domain response of linear hysteretic systems to deterministic and random excitations. *Earthquake Engineering and Structural Dynamics* 2005; **34**:1129–1147.
21. Palmeri A, Ricciarelli F. Fatigue analyses of buildings with viscoelastic dampers. *Journal of Wind Engineering and Industrial Aerodynamics* 2006; **94**:377–395.
22. Palmeri A. Correlation coefficients for structures with viscoelastic dampers. *Engineering Structures* 2006; **28**:1197–1208.
23. Muscolino G, Palmeri A. Response of beams resting on viscoelastically damped foundation to moving oscillators. *International Journal of Solids and Structures* 2007; **44**:1317–1336.
24. Palmeri A. Toward overcoming the concept of effective stiffness and damping in the analysis and design of viscoelastically damped structures. In *Trends in Civil and Structural Engineering Computing*, Topping BH, Costa Neves LF Barros RC (eds). Saxe-Coburg Publications: Stirlingshire, 2004; 267–292.
25. Aprile A, Benedetti A. Implicit dynamic analysis of VE-damped structures using Maxwell parallel systems. *Engineering Computations* 1999; **16**:374–396.
26. Newmark MN. A method of computation for structural dynamics. *Journal of the Engineering Mechanics Division* 1959; **85**:67–94.
27. Patlashenko I, Givoli D, Barbone P. Time-stepping schemes for systems of Volterra integro-differential equations. *Computer Methods in Applied Mechanics and Engineering* 2001; **190**:5691–5718.
28. Hilber HM, Hughes TJR, Taylor RL. Improved numerical dissipation for time integration algorithms in structural dynamics. *Earthquake Engineering and Structural Dynamics* 1977; **5**:283–292.
29. Palmeri A, Ricciarelli F, De Luca A, Muscolino G. State space formulation for linear viscoelastic dynamic systems with memory. *Journal of Engineering Mechanics* 2003; **129**:715–724.

DOI: 10.1002/stc

30. Adhikari S, Wagner N. Analysis of asymmetric nonviscously damped linear dynamic systems. *Journal of Applied Mechanics* 2003; **70**:885–893.
31. Wagner N, Adhikari S. Symmetric state-space method for a class of nonviscously damped systems. *AIAA Journal* 2003; **41**:951–956.
32. Inaudi JA, Kelly JM. Modal equations of linear structures with viscoelastic dampers. *Earthquake Engineering and Structural Dynamics* 1995; **24**:145–151.
33. Orbey N, Dealy JM. Determination of the relaxation spectrum from oscillatory shear data. *Journal of Rheology* 1991; **35**:1035–1049.
34. Syed Mustapha SMFD, Phillips TN. Dynamic nonlinear regression method for the determination of the discrete relaxation spectrum. *Journal of Physics D*: *Applied Physics* 2000; **33**:1219–1229.
35. Caughey TK, O'Kelly MEJ. Classical normal modes in damped linear systems. *Journal of Applied Mechanics*, *Transactions of the ASME* 1965; **32**:583–588.
36. Szidarovszky F, Bahill AT. *Linear Systems Theory* (2nd edn). CRC Press: Boca Raton, 1998.
37. Borino G, Muscolino G. Mode-superposition methods in dynamic analysis of classically and nonclassically damped linear systems. *Earthquake Engineering and Structural Dynamics* 1986; **14**:705–717.
38. Muscolino G. Dynamically modified linear structures: deterministic and stochastic response. *Journal of Engineering Mechanics* 1996; **122**:1044–1051.
39. Kirsch U. A unified reanalysis approach for structural analysis, design, and optimization. *Structural and Multidisciplinary Optimization* 2003; **25**:67–85.
40. Muscolino G, Cacciola P. Re-analysis techniques in structural dynamics. In *Progress in Computational Structures Technology*, Topping BHV, Mota Soares CA (eds). Saxe-Coburg Publications: Stirling, 2004; 31–58.
41. Reddy JN. *An Introduction to the Finite Element Method* (3rd edn). McGraw-Hill: New York, 2007.
42. Mathematica [computer program], release 6.0, Wolfram Research: Champaign, 2007.
43. Fu Y, Kasai K. Comparative study of frames using viscoelastic and viscous dampers. *Journal of Structural Engineering* 1998; **124**(5):513–522.
44. Hiemenz GJ, Choi YT, Wereley NM. Seismic control of civil structures utilizing semi-active MR braces. *Computer-Aided Civil and Infrastructure Engineering* 2003; **18**:31–44.
45. Adhikari S, Pascual B. Eigenvalues of linear viscoelastic systems. *Journal of Sound and Vibration* 2009; **325**:1000–1011.

DOI: 10.1002/stc